Supplementary Information (SI) for RSC Sustainability.
This journal is © The Royal Society of Chemistry 2025

Sustainable Remanufacturing of Mesoscopic Carbon Perovskite Solar Cells Using Green Solvents

Karen Valadez-Villalobos,[a] Carys Worsley [a] Rodrigo Garcia Rodriguez, [a] Trystan Watson[a] and Matthew Davies[ab]

[a] SPECIFIC IKC, Materials Science and Engineering, Faculty of Science and Engineering, Swansea University, Swansea, UK
[b] School of Chemistry and Physics, University of KwaZulu-Natal, Durban, South Africa

SUPPLEMENTARY INFORMATION

Methods.

Materials: PbI_2 (99%, Sigma-Aldrich), MAI (CH_3NH_3I, anhydrous, Dyesol), 5-ammonium valeric acid iodide (5-AVAI, Dyesol), γ-valerolactone (GVL, Sigma Aldrich) were used as received. For device stacks, titanium diisopropoxide bis (acetylacetonate) (TAA, 75% in IPA, Sigma-Aldrich), anhydrous 2-propanol (IPA, 99.5%, Sigma Aldrich), TiO_2 paste (30NR-D, GreatCell Solar), ZrO_2 paste (GreatCell Solar), carbon paste (Gwent electronic materials).

Device Fabrication: FTO substrates were patterned with a Nb:YVO4 laser (532 nm) before cleaning with Hellmanex (Vol 2% in deionized water), rinsing with acetone and IPA, and drying with N_2. Substrates were then plasma cleaned for 5 min in an O_2 environment. A compact TiO_2 blocking layer was deposited by spray pyrolysis of titanium di-isopropoxide-bis(acetylacetonate) (0.2 M) in isopropanol on a hot plate at 300°C. To form the mesoporous TiO_2 layer, the titania paste 30NRD was diluted 1:1 by weight in terpineol, screen printed and sintered at 550°C for 30 min after a slow ramp. Next, ZrO_2 and carbon were printed and annealed at 400°C for 30 min each. All layers were printed and annealed in ambient conditions.

After carbon annealing, devices were cooled before drop casting of the room-temperature precursor (20 µL, 0.95 M) $MAPbI_3$ with 3% molar excess 5-AVAI in a vol 9:1 mixture of GVL and methanol. Devices were left for 15 min in ambient conditions after drop casting to ensure adequate infiltration, before annealing on a hot plate for 1.5 h at 40°C. Solder contacts were applied using an ultrasonic soldering iron at 190°C. Testing on infiltrated devices was performed 4 days after completion.

Remanufacturing.

Remanufacturing of non-aged devices: Two days after the initial infiltration of AVA-MAPI into a new batch of carbon-based devices, and prior to contact soldering, samples were immersed in either 1.5 M aqueous KOH or GVL to remove the perovskite absorber and enable reinfiltration. Each sample was immersed for 15 minutes at room temperature using 50 mL of the respective solvent. KOH-treated samples were subsequently rinsed with deionized water to remove residual base. All rinsed samples (KOH and GVL) were then dried at room temperature for 30 minutes, followed by thermal treatment at 350 °C for 30 minutes to ensure complete solvent removal. After cooling to room temperature, the recovered stacks were immediately reinfiltrated with fresh AVA-MAPI solution. Results were compared against control samples from the same batch that did not undergo reinfiltration. Contacts were soldered one day prior to performance measurement, and power conversion efficiency was recorded for all devices on day 4 after infiltration.

Remanufacturing of aged devices: Devices previously stored under ambient conditions were recovered using a GVL-based rinsing and reinfiltration protocol (Figure S6). To optimize recovery conditions, samples were immersed in GVL at different temperatures (25 °C, 60 °C, and 85 °C) and for varying durations (15, 30, and

60 minutes), using 50 mL of solvent per sample. Following immersion, the devices were dried and reinfiltrated with fresh AVA-MAPI to restore photovoltaic performance.

Characterisation: Devices with a 1 cm^2 active area were masked to 0.16 cm^2 for testing. Current–voltage (J–V) measurements were carried out using a class AAA solar simulator (Newport Oriel Sol3A), calibrated to 1 sun (AM 1.5G, 100 $mW\,cm^{-2}$) with a KG5-filtered silicon reference cell (Newport Oriel 91150-KG5). Devices were scanned in both forward and reverse directions at a rate of 100 $mV\,s^{-1}$ over a voltage range of −0.2 V to 1.1 V, following a 180-second light soaking period.

PL and TRPL measurements were conducted on complete devices, with excitation incident through the glass substrate, thereby illuminating the TiO_2 mesoporous scaffold side of the stack. Steady-state photoluminescence (PL) measurements were carried out using an FS5 spectrofluorometer (Edinburgh Instruments) over a wavelength range of 690–850 nm. Samples were excited at 450 nm, with a 445 nm bandpass filter placed in the excitation path and a 496 nm longpass filter in the emission path. Time-resolved photoluminescence (TRPL) measurements were performed using an FLS1000 photoluminescence spectrometer (Edinburgh Instruments). Samples were excited with an EPL405 pulsed diode laser (λ_{exc} = 405 nm), and emission was collected at 775 nm using a 30 nm emission slit width. The laser repetition period was set to 200 ns. TRPL decay curves were fitted using a bi-exponential model to extract the trap-mediated (τ_1) and radiative (τ_2) recombination lifetimes.

The EL images were taken with a modified Canon EOS 600D camera without IR filters in the dark while a constant voltage was applied to the devices with a RS Pro Bench

Power Supply. The measurements were obtained after applying a Voltage of 1.5 V and an exposition time of 30 seconds.

A

Device	PCE (%)	V_{OC} (V)	Fill Factor (%)	J_{SC} (mA/cm^2)
STD 1-REV	**12.1**	**0.99**	**53**	**22.9**
STD 1-FWD	11.9	0.96	55	23.0
STD 2-REV	**10.0**	**0.99**	**44**	**22.6**
STD 2-FWD	9.9	0.96	45	22.8
GVL-1-REV	**10.7**	**0.99**	**48**	**22.5**
GVL-1-FWD	10.2	1.03	45	22.2
GVL-2-REV	**8.4**	**0.85**	**46**	**21.6**
GVL-2-FWD	8.2	0.86	43	22.2
GVL-3-REV	**8.7**	**0.83**	**46**	**22.8**
GVL-3-FWD	8.4	0.84	44	22.9
GVL-4-REV	**6.4**	**0.94**	**45**	**15.1**
GVL-4-FWD	6.5	0.93	44	15.8
KOH-1-REV	**9.1**	**0.94**	**50**	**19.2**
KOH-1-FWD	3.1	0.81	23	16.1
KOH-2-REV	**8.0**	**0.93**	**51**	**16.8**
KOH-2-FWD	3.6	0.92	33	11.9
KOH-3-REV	**8.8**	**0.93**	**57**	**16.9**
KOH-3-FWD	4.0	0.87	35	13.1
KOH-4-REV	**6.4**	**0.95**	**54**	**12.4**
KOH-4-FWD	3.3	0.93	34	10.3

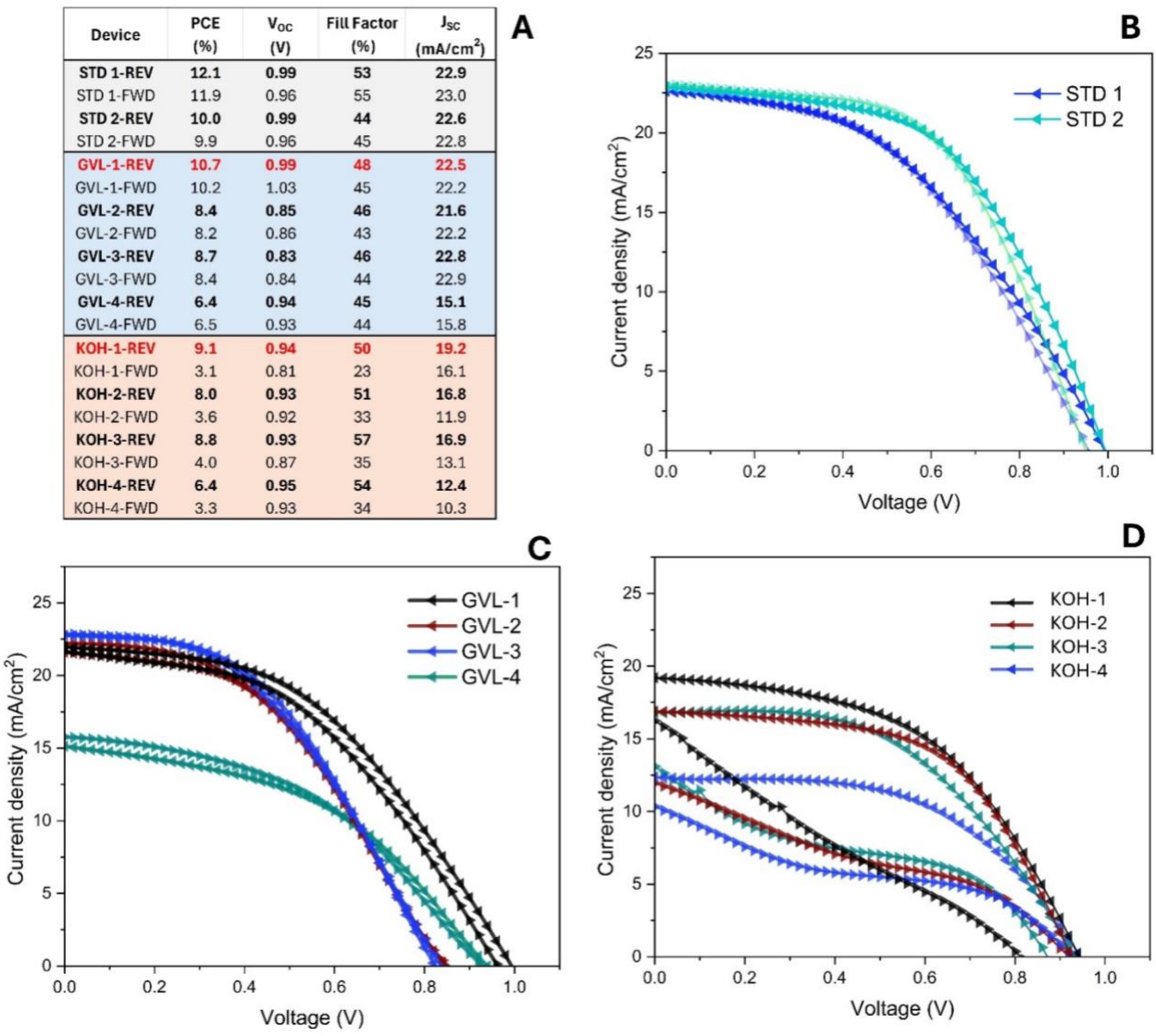

Figure S1. (A) Photovoltaic performance parameters for standard (STD) non-reinfiltrated devices, as well as GVL-rinsed and KOH-rinsed reinfiltrated non-aged devices, measured under reverse (REV) and forward (FWD) scan directions. (B) Current density–voltage (J–V) curves for standard non-reinfiltrated devices. (C) J–V curves for GVL-rinsed reinfiltrated devices. (D) J–V curves for KOH-rinsed reinfiltrated devices.

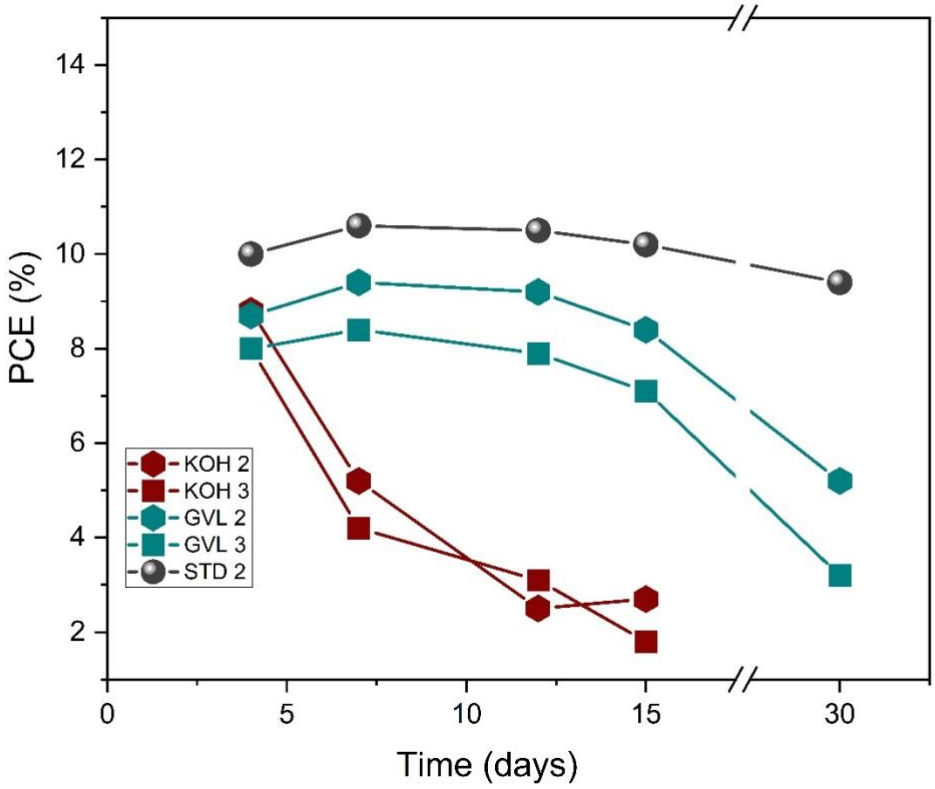

Figure S2. Power conversion efficiency (PCE) evolution over time for GVL- and KOH-rinsed reinfiltrated devices (GVL-2, GVL-3, KOH-2, and KOH-3), compared with the standard non-reinfiltrated device (STD-2). Devices were monitored over a 30-day period to assess stability under ambient conditions.

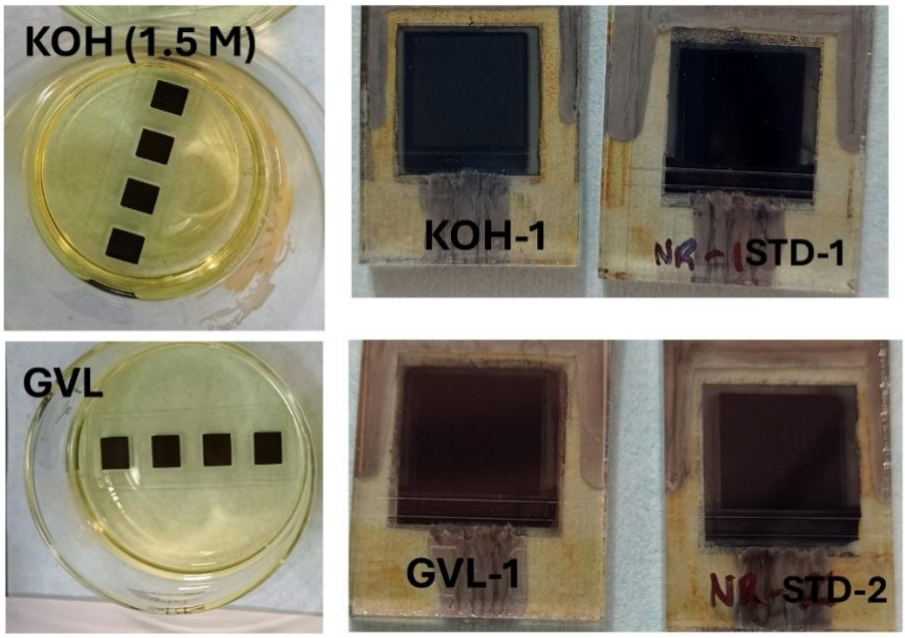

Figure S3. Visual comparison of the rinsing process using KOH (1.5 M) and GVL solvents on non-aged devices (left), alongside the appearance of the best-performing reinfiltrated devices (KOH-1 and GVL-1) compared with their standard non-reinfiltrated devices (STD-1 and STD-2) (right).

Figure S4. Visual comparison of aged devices after rinsing with GVL (left) and KOH (1.5 M) (right). After drying at 350°C, devices rinsed with KOH exhibit a cloudy and uneven appearance, suggesting possible ineffective removal of the AVA-MAPI or residue formation, whereas GVL-rinsed devices retain a more uniform and intact surface.

Figure S5. The integrity of the carbon counter electrode was likely a key factor contributing to the high variability in device performance after recovery. While moderate damage to the carbon film in aged devices had no noticeable effect on first-life efficiency, visible surface imperfections interfered with uniform perovskite removal throughout the stack, often resulting in samples unsuitable for reinfiltration.

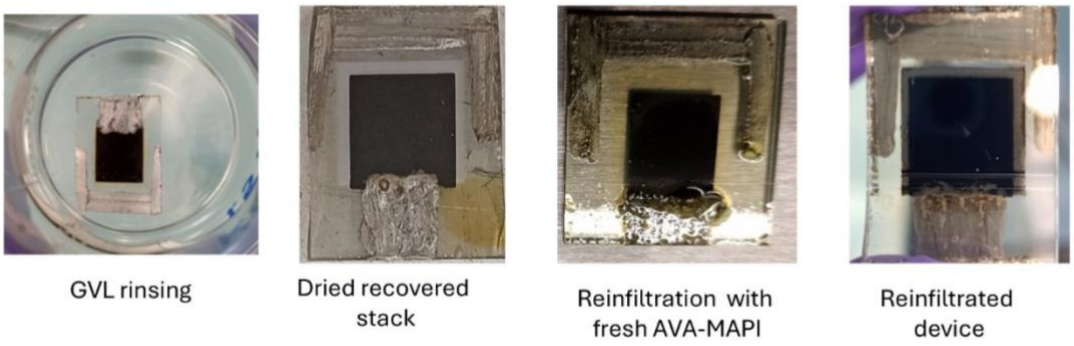

Figure S6. Sequential steps in the GVL-based recovery and reinfiltration process. From left to right: (1) device undergoing GVL rinsing, (2) dried recovered stack after solvent removal, (3) reinfiltration of the stack with fresh AVA-MAPI precursor solution, and (4) final reinfiltrated device.

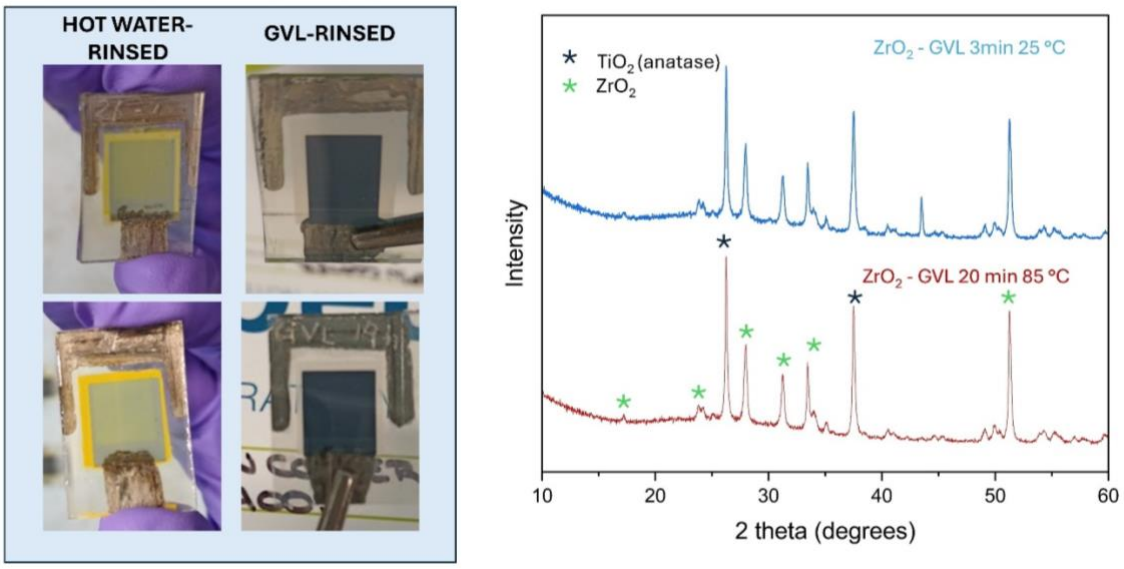

Figure S7. Comparison of perovskite removal after rinsing with hot water (80 °C) and γ-valerolactone (GVL), and XRD analysis of the underlying scaffold after rinsing with GVL. **(Left)** Visible yellow PbI_2 residues after rinsing with hot water (80 °C), contrasted with the absence of visible lead species in the GVL-rinsed sample. **(Right)** XRD diffractograms of GVL-rinsed samples treated under different conditions (3 min at 25 °C and 20 min at 85 °C). The carbon layer was manually removed prior to measurement to expose the mesoporous scaffold. Detected peaks correspond to TiO_2 (anatase) and ZrO_2, with no detectable PbI_2 peaks, confirming effective removal of the absorber layer under both rinsing conditions.

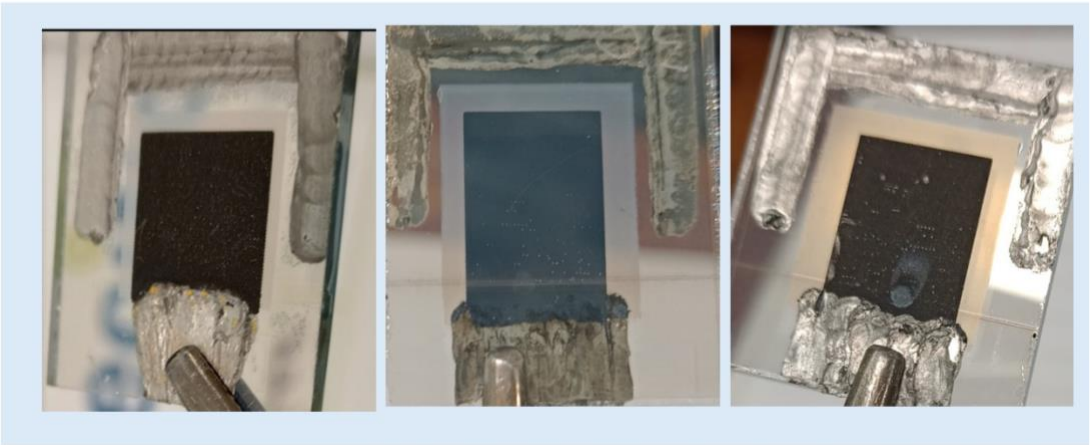

Figure S8. Photographs of substrates recovered using aqueous KOH solution. Even the best-preserved samples display white residues and surface irregularities visible both on top of the carbon layer and visible through the glass side. These features are interpreted as evidence of partial scaffold alteration or diffusion of inner stack materials during alkali treatment.